Available online at www.sciencedirect.com
SCIENCE DIRECT®
Journal of Nuclear Materials 345 (2005) 1–10
journal of nuclear materials
www.elsevier.com/locate/jnucmat

Ex-reactor corrosion and oxide characteristics of Zr–Nb–Fe alloys with the Nb/Fe ratio

Hyun-Gil Kim *, Jeong-Yong Park, Yong-Hwan Jeong

Zirconium Fuel Cladding Team, Korea Atomic Energy Research Institute, 150, Doekjin-dong, Yuseong-gu, Daejeon 305-353, Republic of Korea

Received 7 January 2005; accepted 13 April 2005

Abstract

The effects of different Nb and Fe addition ratios on the microstructure, corrosion and oxide characteristics of Zr-based alloys were investigated. The Nb/Fe ratio was controlled to be 0.6, 1.0, 1.7, 3.0, and 7.0 with the same amount of Nb + Fe in each alloy. The microstructural analysis and precipitate characterization were performed to obtain the correlation between the corrosion and the microstructures. The grain size and the area fraction of the precipitate in all the tested alloys were almost the same even though the Nb/Fe ratio was considerably changed. But the mean diameter and the crystal structure of the precipitates were affected by the variation of the Nb/Fe ratio. In the alloy with a low Nb content, the FCC-$(ZrNb)_2Fe$ precipitate was mainly formed while the HCP-$Zr(NbFe)_2$ precipitate was frequently observed in the alloy of with a high Nb content. The corrosion resistance of the Zr–xNb–yFe ternary alloys was improved by decreasing the Nb/Fe ratio. From the microstructure and corrosion studies, it seems that the corrosion resistance would be more closely related to the crystal structure of the precipitate rather than the other properties such as the size distribution and the density of the precipitates.

1. Introduction

The corrosion resistance of fuel claddings has been considered to be one of the key properties for controlling the performance and the safety of nuclear fuel. Zr-based alloys have been used as fuel cladding materials and a great number of researches have been done to improve the corrosion resistance of the Zr-based alloys. The development of advanced cladding materials with an improved corrosion resistance has been extensively carried out in many countries operating nuclear power plants for the last few decades [1–3]. They have reported that the corrosion kinetics of Zr-alloy were affected by the alloying element and the precipitates that are formed by various alloying elements when there was an excess soluble limit in α-Zr. Among the various alloying elements, Nb and Fe are considered to be very effective for improving the corrosion resistance of the Zr-based alloys [1,2]. It has been reported that the corrosion resistance of the Zr alloys was improved when the Nb was added at a range less than the solubility of the α-Zr. Even though the Nb content is higher than the solubility of α-Zr, the Zr alloys showed a better corrosion

* Corresponding author. Tel.: +82 42 868 2522; fax: +82 42 862 0432.
E-mail address: hgkim@kaeri.re.kr (H.-G. Kim).

0022-3115/$ - see front matter © 2005 Elsevier B.V. All rights reserved.
doi:10.1016/j.jnucmat.2005.04.061

resistance when β-Nb precipitates are formed by a heat-treatment below the monotectoid temperature [3]. It has also been reported that Fe improved the corrosion resistance of the Zr alloys when added at a range more than 0.2 wt% [4].

The precipitate types are determined by some kinds of alloying elements and annealing conditions. It is known that in Zircaloy-type alloys, the precipitates size was a very sensitive parameter for the corrosion resistance [4] and the effects of the Fe/Cr ratio in the precipitate on the corrosion resistance have been extensively investigated [5]. From the study of the second phase particles in a Zr binary alloy, an improvement in the corrosion behavior at a high temperature can be obtained by a higher volume fraction and size of the intermetallic precipitates [6].

Although Nb and Fe are considered to be important alloying elements in the advanced Zr-based alloys, the effect of the Nb/Fe ratio on the precipitate characteristics and the corrosion behavior was not evaluated in the Nb-containing Zr alloys. The aim of this study is to investigate the effect of the Nb/Fe ratio on the corrosion of the Zr alloys. Microstructure observations, a corrosion test and an oxide characterization were performed for the Zr–Nb–Fe ternary alloys with various addition ratios of Nb/Fe.

2. Experimental procedure

The experimental alloys with various Nb/Fe ratios were manufactured to investigate the optimum ratio for the corrosion. As shown in Table 1, the Nb content ranged from 0.3 to 0.7 wt% and the Fe content ranged from 0.1 to 0.7 wt% in the Zr–*x*Nb–*y*Fe ternary alloys. The Nb/Fe ratio was controlled by decreasing the Nb content with an increasing Fe content so that the total amount of Nb + Fe content in wt% was the same in all of the alloys although the total amount of that in at.% was slightly decreased. The lowest Nb content (0.2 wt%) selected in this study was the critical Nb content to form the Nb-containing precipitates which was observed in our previous study [7]. The addition ratio of Nb/Fe in the experimental alloys was controlled to be 0.6, 1.0, 1.7, 3.0 and 7.0.

The experimental alloys were manufactured by the sequence of a vacuum arc melting (4 times), water-quenching after β-solution treatment at 1020 °C for 30 min, hot rolling (60% reduction in thickness) after pre-heating at 570 °C for 30 min and then 3 times cold rolling (50% reduction in thickness). The cold-rolled sheets were annealed at 570 °C for 3 h after each cold rolling step. To focus on the effects of the precipitate characteristics on the corrosion, the microstructures of the alloys were controlled to have a recrystallized structure whose grain size was almost similar in all of the alloys. The Nb/Fe ratio in the precipitates was analyzed using a transmission electron microscope (TEM) equipped with an energy dispersive X-ray spectroscopy (EDS). The area fraction and the mean diameter of the precipitates were calculated using an image analyzer. The samples for the TEM observation were prepared by a twin jet polishing method after a mechanical thinning to about 70 μm.

The corrosion test was performed in a static autoclave of 360 °C water under a saturation pressure of 18.9 MPa. The corrosion resistance was evaluated by measuring the corrosion weight gain of the corroded samples after suspending the corrosion test at a periodic term.

The small angle X-ray diffraction and the cross-sectional TEM method were used to analysis the oxide characteristics. The fraction of the tetragonal ZrO_2 was calculated for the pre-transition oxide having an equal oxide thickness of different Nb/Fe ratio alloys, and the microstructure of the oxide and the precipitates in the oxide were observed for the post-transition oxide having an equal corrosion time of 350 days.

3. Results and discussion

3.1. Microstructures and the precipitates characteristics

The optical microstructure and the grain size of the final-annealed alloy are shown in Fig. 1. Each alloy

Table 1
Model alloy composition and Nb/Fe ratio of the Zr–Nb–Fe ternary system

Sample	Nb (wt%)	Fe (wt%)	Nb + Fe		Nb + Fe at.% available for precipitate	Nb/Fe ratio	
			(wt%)	(at.%)		(wt%)	(at.%)
1	0.3	0.5	0.8	1.11	0.91	0.6	0.36
2	0.4	0.4	0.8	1.04	0.84	1.0	0.61
3	0.5	0.3	0.8	0.98	0.78	1.7	1.02
4	0.6	0.2	0.8	0.92	0.72	3.0	1.83
5	0.7	0.1	0.8	0.85	0.65	7.0	4.29

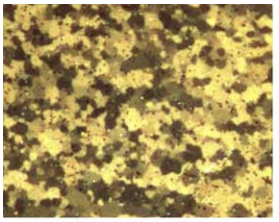

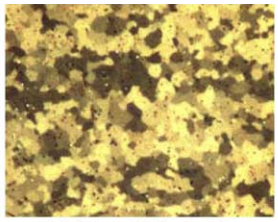

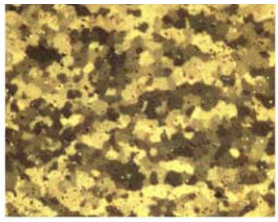

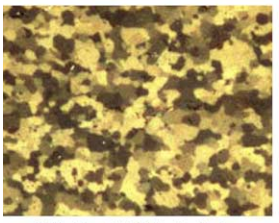

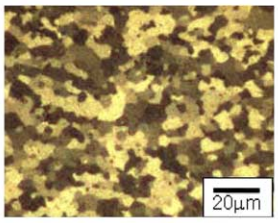

Alloy	Grain size (μm)
(a)	4.2
(b)	4.5
(c)	4.3
(d)	4.6
(e)	4.7

Fig. 1. Optical microscopy and grain size of the Zr–Nb–Fe alloys.

was shown to have a recrystallized structure with equiaxed grains and the measured grain size ranged from 4.2 to 4.7 μm depending on the alloy composition. However, the difference of the grain size in the alloys was not significant although the alloys had a variety of Nb/Fe ratios. Fig. 2 shows the TEM microstructure of the second phase particles in the alloys. Precipitates with various sizes were uniformly distributed in the grain as well as the grain boundaries.

The size distribution, the mean diameter and the area fraction of the observed precipitates are shown in Fig. 3. For reducing the calculation errors, the TEM micrographs taken from different grains in the same alloy were selected to analyze the precipitate characteristics. The parameters such as the mean diameter and the area fraction were determined from the analysis on the precipitates of more than 350 e.a. Although the alloy composition was greatly altered, the area fraction of the precipitate was slightly decreased with an increasing Nb/Fe ratio.

From the view point of the model alloy design, it was intended to obtain a similar amount of precipitate in all the alloys by adding the same content of Nb and Fe in each alloy. It has been reported that the solubility of the Nb in α-Zr was about 0.2 wt% [7] and that of Fe was 100 ppm [8]. Therefore, all the ternary alloys designed in this study have almost a similar amount of the precipitate of Nb and Fe in the matrix. The size distribution of the precipitate was changed with the Nb/Fe addition ratio. As the Nb/Fe ratio increased, the mean diameter of the precipitate decreased from 62.98 nm to 38.31 nm as shown in Fig. 3. This implies that the precipitate mean diameter is strongly affected by the Nb/Fe ratio.

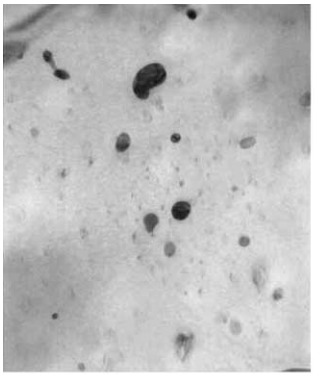

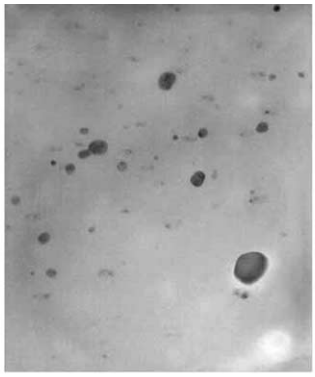

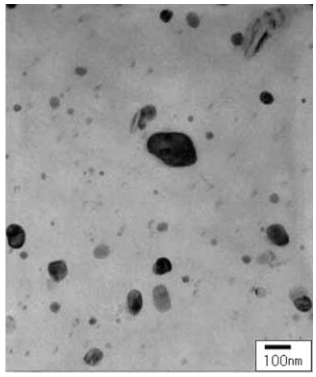

Fig. 2. TEM microstructure of the precipitates distribution in the alloys.

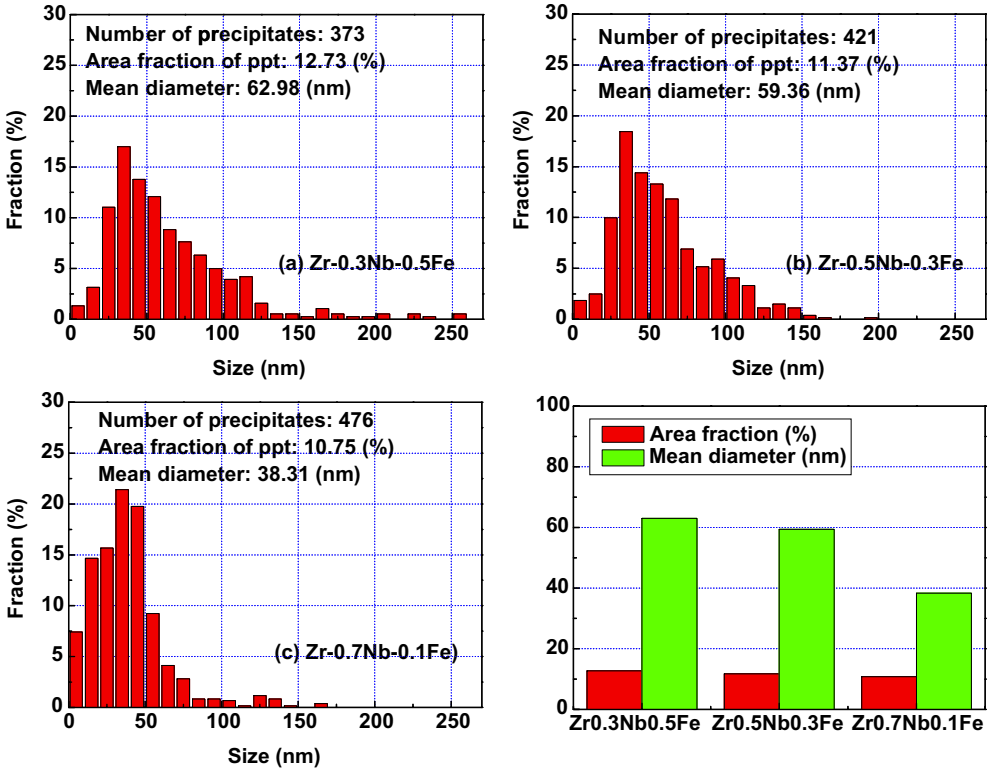

Fig. 3. Size distribution, mean diameter and area fraction of the observed precipitates.

The crystal structure and chemical composition of the precipitate were analyzed using a TEM equipped with EDS. To increase the reliability of the analysis, the number of encountered precipitates was more than 30 for each alloy. From the precipitates analysis, $(ZrNb)_2Fe$ precipitate of a FCC structure having a composition of about 64 at.%Zr–16 at.%Nb–20 at.%Fe was mainly observed at a lower Nb/Fe ratio than 1.0. and $Zr(NbFe)_2$ precipitate of a HCP structure having a composition of about 45 at.%Zr–30 at.%Nb–25 at.%Fe was mainly observed in the alloy with a higher Nb/Fe ratio. The crystal structure of the precipitate was critically changed between 1.0 and 1.7 for the Nb/Fe ratio. Similar results to this observation have been reported in previous studies [9]. The precipitate characteristics are summarized in Table 2. The main precipitates in the investigated alloys were Zr_3Fe, $(ZrNb)_2Fe$ and $Zr(NbFe)_2$. In the alloys with a high Nb content, the HCP $Zr(NbFe)_2$ precipitate was mainly observed while the FCC $(ZrNb)_2Fe$ precipitate was frequently observed in the alloys with a high Fe content. The Zr_3Fe precipitate was observed in all of the alloys even though its

Table 2
The precipitate characteristics of the Zr–Nb–Fe alloys having different Nb/Fe ratios

Alloy (at.% ratio)	Precipitate characteristics			Remark
	Phase type	Structure	Average composition (at.%)	
Zr–0.3Nb–0.5Fe	Zr_3Fe	Ortho (lm-3m)	75Zr–25Fe	Minor
(Nb/Fe ratio: 0.32)	**$(ZrNb)_2Fe$**	**FCC** (Fm-3m)	63Zr–15Nb–22Fe	**Major**
Zr–0.5Nb–0.3Fe	Zr_3Fe	Ortho (lm-3m)	75Zr–25Fe	Minor
(Nb/Fe ratio: 0.73)	$(ZrNb)_2Fe$	FCC (Fm-3m)	64Zr–16Nb–20Fe	Minor
	$Zr(NbFe)_2$	**HCP** (P63/mmc)	45Zr–30Nb–25Fe	**Major**
Zr–0.7Nb–0.1Fe	Zr_3Fe	Ortho (lm-3m)	75Zr–25Fe	Minor
(Nb/Fe ratio: 2.56)	$(ZrNb)_2$ Fe	FCC (Fm-3m)	63Zr–17Nb–20Fe	Minor
	$Zr(NbFe)_2$	**HCP** (P63/mmc)	45Zr–33Nb–22Fe	**Major**

fraction was very low. The β-Nb phase was not observed in this alloy system even in the high Nb content of 0.7 wt% due to the slow diffusion rate of niobium. From the study of the equilibrium condition for β-Nb phase formation, it takes about 50 h of annealing at 570 °C to get the β-Nb phase precipitation [10]. Therefore, it could be thought that the total annealing time was somewhat short to get equilibrium phase in the sample manufacturing process.

3.2. Corrosion and oxide characteristics

The corrosion test at a 360 °C water condition was performed for up to 390 days. Fig. 4 shows the corrosion weight gain as a function of the exposure time and the Nb/Fe ratio. The corrosion resistance was decreased by increasing the Nb/Fe ratio. It was noted that the corrosion resistance was critically changed with the Nb/Fe ratio between 1 and 1.7. The corrosion kinetics was divided into two groups according to the Nb/Fe ratio. When the Nb/Fe ratio is lower than 1.0, the alloys showed a lower corrosion rate than the alloys with a higher Nb/Fe ratio. From the matrix properties, the effect of the matrix composition can be considered to be equivalent in all of the alloys because the contents of Nb and Fe are higher than their solubility in all of the alloys. And the grain size and the precipitate area fraction in the alloys were similar. So, the different corrosion behavior may have resulted from the different precipitate characteristics in the alloys which changed with the Nb/Fe ratio. It has been reported from a recent study on the corrosion of the ternary Zr–Nb–Fe system that the corrosion behavior in steam significantly depended on the SPP volume fraction [11]. In this study, however, the corrosion behavior of the alloys was shown to be different from the previous results.

Fig. 5 shows the corrosion behavior versus the microstructural characteristics with the Nb/Fe ratio of the alloys. The corrosion rate was drastically changed with the Nb/Fe ratio between 1 and 1.7, but the other microstructural characteristics were not greatly changed with the Nb/Fe ratio. The mean grain size and the precipitate area fraction were almost the same and the precipitate mean diameter was decreased by increasing the Nb/Fe ratio. From the result of the precipitate analysis, the FCC $(ZrNb)_2Fe$ precipitates were mainly formed at a low Nb/Fe ratio while the HCP $Zr(NbFe)_2$ precipitates were mainly formed at a high Nb/Fe ratio. The lower corrosion rate was observed when the $(ZrNb)_2Fe$ precipitates were formed in the alloys with a lower Nb/Fe ratio than 1.0. The $(ZrNb)_2Fe$ precipitate seems to be more beneficial for improving the corrosion resistance than the $Zr(NbFe)_2$ in the ternary Zr–*x*Nb–*y*Fe alloy. Therefore, it could be assumed that the corrosion rate of the Zr–*x*Nb–*y*Fe alloys is more strongly affected by the precipitate type rather than the other characteristics of the precipitates and the grain size.

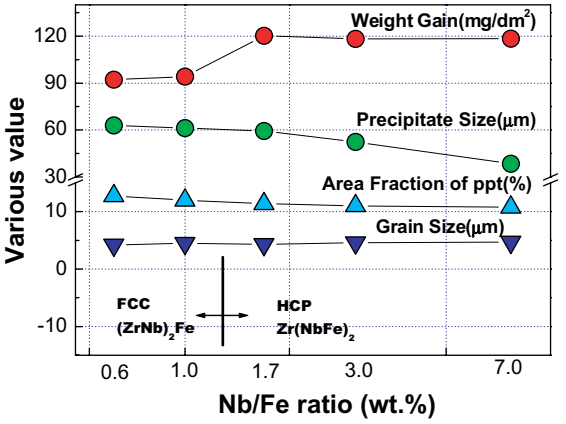

Fig. 5. Corrosion behavior versus the microstructural characteristics with the Nb/Fe ratio of the alloys.

From the oxide analysis of the crystal structure as shown in Fig. 6, the tetragonal ZrO_2 phase and monoclinic ZrO_2 phase peaks were observed for the pre-transition oxide having an equal oxide thickness of the

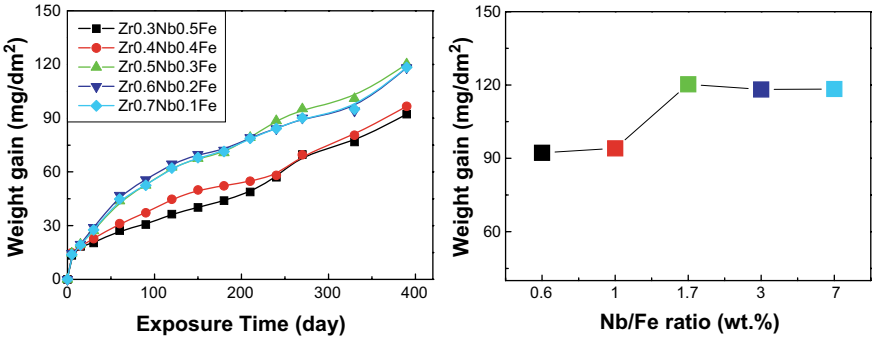

Fig. 4. Corrosion behavior of the Zr–Nb–Fe alloy at a 360 °C water condition for 390 days.

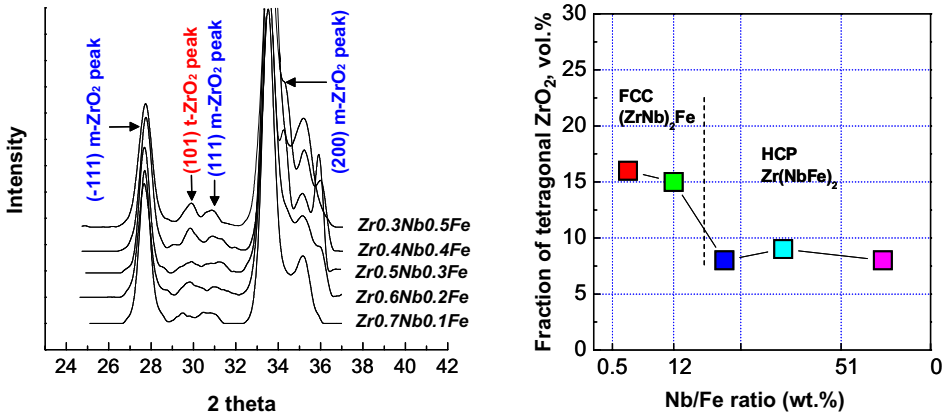

Fig. 6. Small angle X-ray diffraction spectra of the Zr–Nb–Fe alloys and the fraction of the tetragonal phase with the Nb/Fe ratio.

different Nb/Fe ratio alloys. The volume fraction of the tetragonal ZrO_2 phase was higher in the oxide that was formed in the low Nb/Fe ratio alloy. Especially, the correlation between the corrosion behavior and the tetragonal fraction is well matched with the Nb/Fe ratio. Therefore, it is suggested that the tetragonal ZrO_2 phase would be more easily stabilized by the precipitation of FCC $(ZrNb)_2Fe$ than HCP $Zr(NbFe)_2$ in the Zr–*x*Nb–*y*Fe alloy.

Fig. 7 shows the shape of the oxide–metal interface for the post-transition region of the oxide corroded for 330 days. A uniform interface was formed for the low Nb/Fe ratio alloy having the FCC $(ZrNb)_2Fe$ precipitate in the matrix, but the wavy interface was formed at the high Nb/Fe ratio alloy having the HCP $Zr(NbFe)_2$ precipitate in the matrix. Also, lateral cracks were observed in the oxide having a wavy interface. The difference of the oxide–metal interface shape resulted from the different oxide growth rate depending on the discrete oxygen diffusion rate with the local area of the oxide. Generally, good corrosion resistant alloys show a uniform oxide–metal interface but bad corrosion resistant alloys show an irregular interface due to the oxide characteristics that have a locally non-protective area in the oxide.

The morphology of the oxide microstructure is shown in Fig. 8. Fig. 8(a) shows the TEM oxide microstructure prepared for the post-transition region of the Zr–0.3Nb–0.5Fe alloy which showed a good corrosion resistance. In the low Nb/Fe ratio alloy, the oxide morphology mainly consisted of a columnar structure except for the outer part which was mixed with some equiaxed structures. The shape of the columnar structure near the metal–oxide interface was very dense. Fig. 8(b) shows the TEM oxide microstructure prepared for the post-transition of the Zr–0.7Nb–0.1Fe alloy having a lower corrosion resistance than the Zr–0.3Nb–0.5Fe alloy. The oxide morphology of the Zr–0.7Nb–0.1Fe alloy also consisted of a columnar and an equiaxed structure, but the outer part of oxide had a higher equiaxed structure fraction than that of the oxide in the Zr–0.3Nb–0.5Fe alloy. Because the metal–oxide interface of the columnar structure in the Zr–0.7Nb–0.1Fe alloy had a more

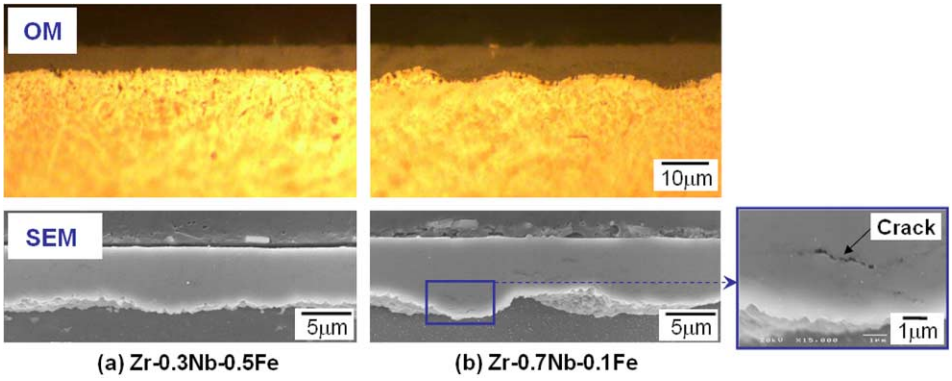

Fig. 7. Oxide–metal interface of the post-transition region of the oxide corroded for 330 days.

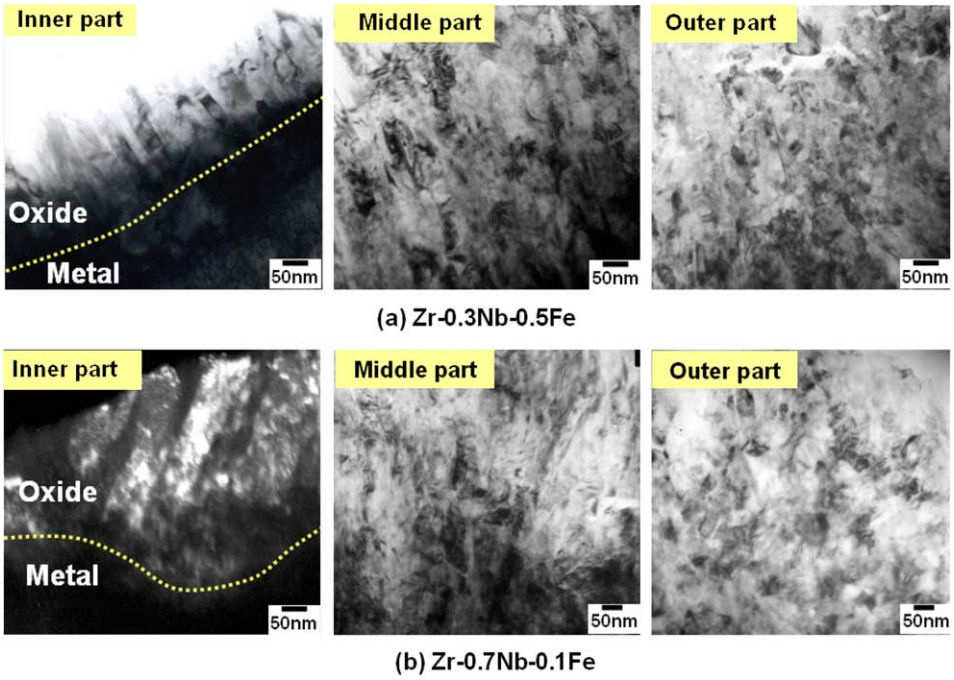

Fig. 8. TEM microstructure of the post-transition oxide corroded for 390 days.

irregular shape than that of the columnar structure in the Zr–0.3Nb–0.5Fe alloy, the oxidation characteristics of a low Nb/Fe ratio alloy were different when compared to that of a high Nb/Fe ratio alloy. Generally, a good corrosion resistance alloy contains more columnar structures in the oxide, at a long distance from the oxide–metal interface [12–14]. From this result, it is assumed that another factor for determining the corrosion resistance was the shape of the columnar structure near the metal–oxide interface.

To investigate the evolution process of the precipitates in the oxide, it was attempted to observe the precipitates in the oxide. A few precipitates were observed in the oxide as shown in Figs. 9 and 10 and the observed precipitate was described as two directions of the cross-section and the plan-view. Fig. 9 shows the precipitate in the post-transition oxide of the Zr–0.3Nb–0.5Fe alloy. The observed precipitate in the oxide showed the nanocrystallite characteristics which were confirmed by the diffraction pattern and the observed precipitate composition in the oxide was different when compared to the precipitate composition in the matrix. The difference of the precipitate composition between the oxide and the matrix was caused by the diffusion of the Nb and Fe around the oxide and the diffusion of the oxygen into the precipitate during an oxidation. So, the evolution process of the precipitate was generated by the oxidation. Fig. 10 shows the precipitate in the post-transition oxide of the Zr–0.7Nb–0.1Fe alloy. The observed precipitate in the oxide showed amorphous characteristics which were also confirmed by the diffraction pattern, and the precipitate composition was also changed between in the matrix and in the oxide. The incorporated precipitates in the oxide have been reported in previous studies [13,15], but it was not clearly defined how the different types of precipitate in the oxide were formed. For the reasons mentioned above, it could be assumed that the different crystallographic characteristics of the precipitates in the oxide were closely related to the initial precipitate types of the FCC-$(ZrNb)_2Fe$ or HCP-$Zr(NbFe)_2$.

Fig. 11 shows the composition change of the precipitates between in the matrix and in the oxide. In the FCC precipitate, Zr is slightly decreased but the Nb and Fe is significantly decreased with an oxidation. In the HCP precipitate, Zr is also slightly decreased but the Nb and Fe is decreased less than those of the FCC precipitate. From this result, the diffusion rates of Nb and Fe in the FCC precipitate are faster than those in the HCP precipitate during an oxidation. Also, the Nb/Fe ratio change of precipitate between in the matrix and in the oxide was compared. The Nb/Fe ratio of the FCC precipitate is significantly increased from 0.6 to 1.97, but that of the HCP precipitate is slightly increased from 1.86 to 2.83. This means that the diffusion rate of Fe in the FCC precipitate is faster than that in the HCP precipitate. It could be related to the stability of the precipitate structure during the oxidation. It could be

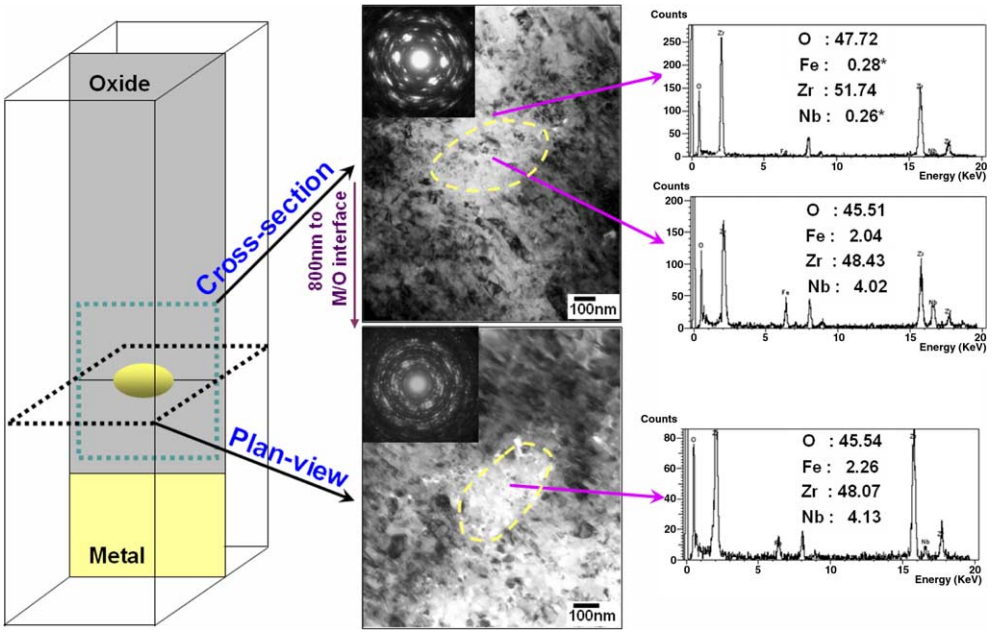

Fig. 9. Cross-sectional and plan-view of the incorporated precipitate in the oxide of the Zr–0.3Nb–0.5Fe alloy.

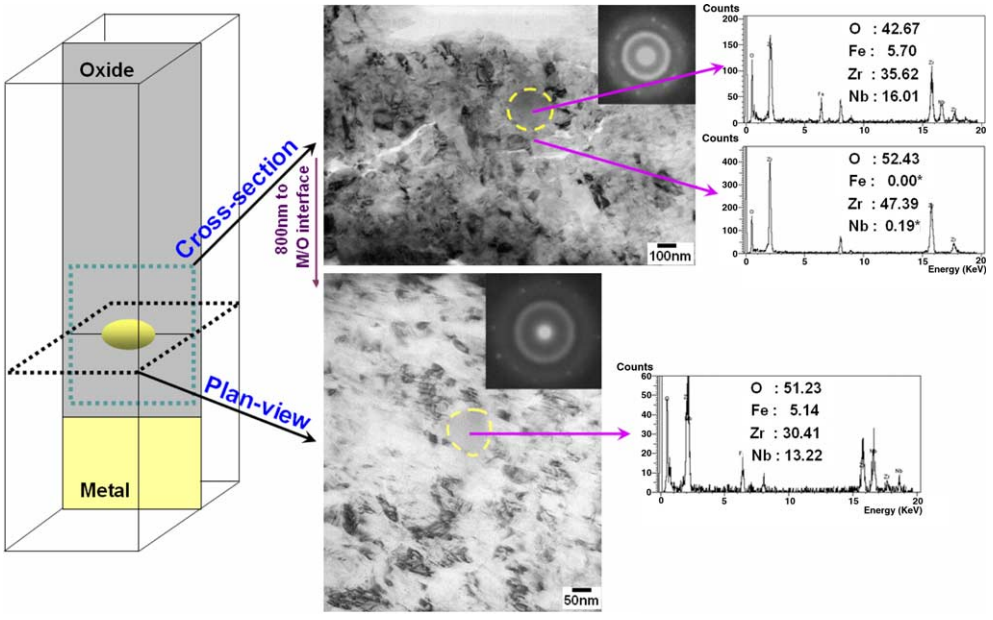

Fig. 10. Cross-sectional and plan-view of the incorporated precipitate in the oxide of the Zr–0.7Nb–0.1Fe alloy.

assumed that the diffusion rate of the elements between the Nb and Fe around the oxide and the diffusion of the oxygen into the precipitate during an oxidation is a main factor for determining the precipitate characteristics of nanocrystallite type or amorphous type in the oxide.

Fig. 12 shows the schematic view of the precipitate evaluation process and the oxide microstructure. In the low Nb/Fe ratio alloy, the major precipitate was the FCC-type which was confirmed by the matrix TEM analysis. This precipitate is changed to a nanocrystallite precipitate with the oxidation progress in the oxide, and

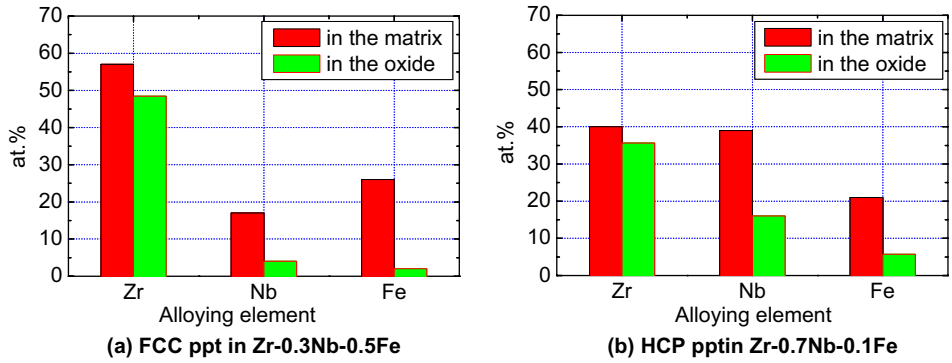

Fig. 11. Composition change of the precipitates between in the matrix and in the oxide.

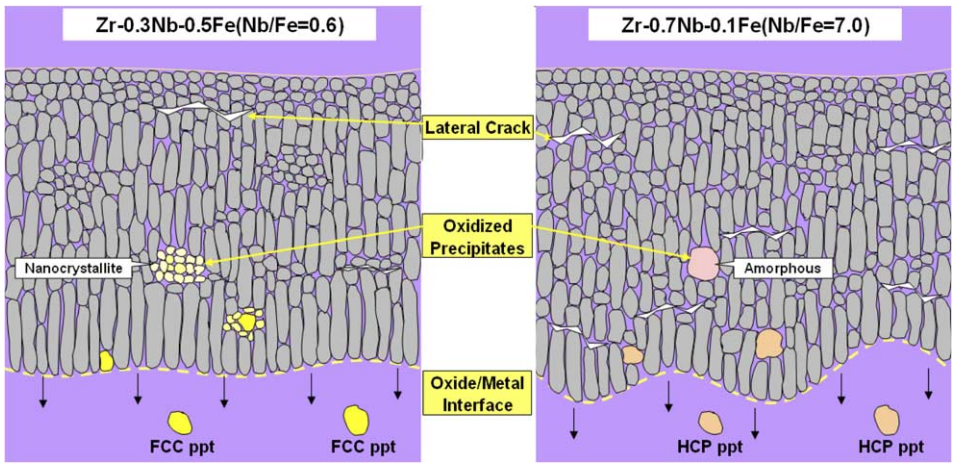

Fig. 12. Schematic view of the precipitate evaluation and oxide microstructure of the post-transition.

then fully oxidized at some distance from the metal–oxide interface. Here, no other precipitate type such as an un-oxidized precipitate and an amorphous precipitate even in near the metal–oxide interface as shown in the left part of Fig. 12 was observed. However, the HCP-type precipitate is changed to an amorphous precipitate in the oxide as shown in the right part of Fig. 12. Here, no other precipitate type was found in the oxide and only the amorphous precipitate in all the areas of the oxide was observed. In this high Nb/Fe ratio alloy, the oxide showed a more irregular metal–oxide interface, shorter columnar grain, and many more lateral cracks than that of the low Nb/Fe ratio alloy. It is suggested that the oxidation rate of the FCC-type precipitate in the oxide is faster than that of the HCP-type precipitate from the results of the EDS analysis.

The corrosion resistance of the Zr alloys was improved when the fraction of tetragonal phase increased in the dense oxide layer near the interface [16]. And the compressive stress gradient in the Zr oxide and correlated the stress build-up with the tetragonal phase stability was measured by using a Raman spectroscopy [17]. From the oxide analysis of the crystal structure as shown in Fig. 6, it was assumed that tetragonal phase fraction was related to the corrosion bebavior. The fast oxidation of FCC-$(ZrNb)_2Fe$ gives rise to the volume change in the oxide. Therefore, this volume change could lead to the formation of a stress field around the precipitate. And the stress field could continuously stabilize the neighboring tetragonal phase in the oxide [16]. Since the transition of corrosion rate was caused by the transformation from a tetragonal to a monoclinic phase in the oxide near the metal–oxide interface, the alloy containing the FCC precipitate shows a good corrosion resistance when compared to that containing the HCP precipitate. However, other recent investigations do not show this trend [18,19]. Yilmazbayhan et al. [18] analyzed the crystal structures of oxides formed on the different Zr alloys (Zircaloy-4, ZIRLO, Zr–2.5Nb and Zr–2.5Nb–0.3Cu) and Park et al. analyzed those of oxides formed on the

Zircaloy-4 and Zr–1.5Nb alloys using a synchrotron radiation. These two studies mentioned that the corrosion behavior was more related to the size of monoclinic phase than the fraction of tetragonal phase. Because the stability of the tetragonal phase can be affected by alloying elements such as Sn [20] and Fe [21], it was necessary that the composition of tested alloys was considered to analyze the correlation on corrosion characteristics and tetragonal phase. In this study, the experimental alloys were manufactured by using the same elements of Zr, Nb and Fe although the amount of that in at.% was different. Therefore, it was suggested that the study for the correlation on tetragonal phase and corrosion behavior was more necessary.

From the view point of the oxide microstructure, it is assumed that the growth of columnar grains is related to the orientation of the tetragonal phase. But, it is necessary to closely study the relationship between the columnar structure orientation and the tetragonal phase which was affected by the precipitate types.

4. Conclusions

The effects of the Nb/Fe ratio on the microstructural characteristics, corrosion behavior and oxide characteristics were investigated for the non-irradiated Zr–Nb–Fe ternary alloys.

In the greatly changed Nb/Fe ratio (0.6–7.0) alloys, the grain size and the area fraction of the precipitate in all the tested alloys were not greatly effected, but the mean size and crystal structure of the precipitates were affected by the variation of the Nb/Fe ratio. The FCC-$(ZrNb)_2Fe$ precipitate was formed in a low Nb/Fe ratio alloy and the HCP-$Zr(NbFe)_2$ precipitate was formed in a high Nb/Fe ratio alloy. The corrosion rate of the Zr–*x*Nb–*y*Fe ternary alloys was considerably changed with the Nb/Fe ratio between 1.0 and 1.7. When the Nb/Fe ratio is lower than 1.0, the alloys showed a lower corrosion rate than the alloys with a higher Nb/Fe ratio. Since a correlation was not found between the corrosion behavior and the precipitate characteristics such as the size and area fraction, it could be more closely related to the crystal structure of the precipitate rather than the other factors. As a study of the precipitate evolution process in oxide, it is suggested that the tetragonal ZrO_2 phase would be more easily stabilized by the formation of the FCC-$(ZrNb)_2Fe$ type precipitate in the matrix for the non-irradiated Zr–*x*Nb–*y*Fe alloys.

Acknowledgement

This study was supported by Korea Institute of Science and Technology Evaluation and Planning (KISTEP) and Ministry of Science and Technology (MOST), Korean government, through its national nuclear technology program.

References

[1] A.V. Nikulina, J. Nucl. Mater. 238 (1996) 205.
[2] R.J. Comstock, G. Schoenberger, G.P. Sabol, ASTM STP 1295 (1996) 710.
[3] Y.H. Jeong, H.G. Kim, T.H. Kim, J. Nucl. Mater. 317 (2003) 1.
[4] F. Garzarolli, H. Stehle, E. Steinberg, ASTM STP 1295 (1996) 12.
[5] C.M. Eucken, P.T. Finden, S. Trapp-Pritsching, H.G. Weidinger, ASTM STP 1023 (1989) 113.
[6] P. Barberis, E. Ahlberg, N. Simic, D. Charquet, C. Lemaignan, G. Wikmark, M. Dahlbäck, M. Limbäck, P. Tägtström, B. Lehtinen, ASTM STP 1423 (2002) 33.
[7] J.Y. Park, Y.S. Kim, H.G. Kim, Y.H. Jeong, in: Proceedings of ENS Top Fuel 2003, Würzburg, Germany, 16–19 March 2003.
[8] R. Borrelly, P. Merle, L. Adami, J. Nucl. Mater. 170 (1990) 147.
[9] C. Toffolon, J.-C. Brachet, C. Servant, L. Legras, D. Charquet, P. Barberis, J.-P. Mardon, ASTM STP 1423 (2002) 361.
[10] H.G. Kim, Y.H. Jeong, T.H. Kim, J. Nucl. Mater. 326 (2004) 25.
[11] P. Barberis, D. Charquet, V. Rebeyrolle, J. Nucl. Mater. 326 (2004) 163.
[12] F. Garzarolli, H. Seidel, R. Tricot, J.P. Gros, ASTM STP 1132 (1991) 395.
[13] H. Anada, B.J. Herb, K. Nomoto, S. Hagi, R.A. Graham, T. Kuroda, ASTM STP 1295 (1996) 74.
[14] Y.H. Jeong, J.H. Back, S.J. Kim, H.G. Kim, H. Ruhmann, J. Nucl. Mater. 270 (1998) 322.
[15] D. Pêcher, J. Nucl. Mater. 278 (2000) 195.
[16] J. Godlewski, ASTM STP 1245 (1994) 663.
[17] J. Godlewski, P. Bouvier, G. Lucazeau, L. Fayette, ASTM STP 1354 (2000) 877.
[18] A. Yilmazbayhan, A.T. Motta, R.J. Comstock, G.P. Sabol, B. Lai, Z. Cai, J. Nucl. Mater. 324 (2004) 6.
[19] J.Y. Park, H.G. Kim, Y.H. Jeong, Y.H. Jung, J. Nucl. Mater. 335 (2004) 433.
[20] P. Li, I.W. Chen, J.E. Penner-Hahn, J. Am. Ceram. Soc. 77 (1994) 1281.
[21] H.-J. Beie, A. Mitwalsky, F. Garzarolli, H. Ruhmann, H.-J. Sell, ASTM STP 1245 (1994) 615.